IEEE Access
Multidisciplinary | Rapid Review | Open Access Journal

Received September 5, 2020, accepted September 22, 2020, date of publication October 19, 2020, date of current version October 29, 2020.

Digital Object Identifier 10.1109/ACCESS.2020.3031969

Speed Regulation Based on Adaptive Control and RBFNN for PMSM Considering Parametric Uncertainty and Load Fluctuation

HONGYU JIE, GANG ZHENG, JIANXIAO ZOU, (Member, IEEE), XIAOSHUAI XIN, AND LUOLE GUO

School of Automation Engineering, University of Electronic Science and Technology of China (UESTC), Chengdu 611731, China

Corresponding author: Hongyu Jie (hyxie_lucas4681@foxmail.com)

This work was supported in part by the National Natural Science Foundation of China under Grant 51707030, and in part by the National Key Research and Fundamental Research Funds for the Central Universities under Grant ZYGX2019Z013.

ABSTRACT A novel speed control scheme combining adaptive speed controller and radial basis function neural network (ASC-RBFNN) is proposed for the speed regulation of permanent magnet synchronous motor (PMSM) in this paper. On one hand, in order to reduce the effect of parametric uncertainty and complicated load fluctuation on the speed control performance, an ASC is proposed. Meanwhile, the speed control system (SCS) of PMSM with the proposed ASC is asymptotically stable even though the parametric uncertainty and complicated load fluctuation exist. On the other hand, with consideration of the uncertainty of complicated load, PMSM parameters, and ASC parameters, the RBFNN is used to optimize all ASC parameters for optimal speed control performance. Finally, the performance is verified on an experiment platform. The results indicate that the SCS with the ASC-RBFNN speed control scheme is with good system stability, fast speed response, and strong anti-fluctuation performance in whole-speed range.

INDEX TERMS Adaptive speed controller, load fluctuation, parametric uncertainty, PMSM, RBFNN.

I. INTRODUCTION

Permanent magnet synchronous motor (PMSM) has been extensively used in industrial applications, such as wind power systems, medical instruments, consumer electronics, robots, and electric vehicles due to its inherent characteristics of small size, simple structure, high reliability, and good torque and speed control characteristics [1]–[3]. In these applications, good speed control performance is important. For the speed control system (SCS) of PMSM, the rotor field-oriented control (FOC) theory has been extensively utilized [4]–[8]. However, the motor parameters, including the moment of inertia (J) and the viscous friction coefficient (B), are uncertain due to various factors, including the inconsistent production, the mechanical wear, the change of the temperature, and the complicated work conditions [9], [10]. Furthermore, there is complicated load fluctuation in the SCS due to the nonlinear friction and complicated work conditions [11], [12]. The parametric uncertainty and complicated load fluctuation lead to poor system stability and large speed fluctuation.

The design of the speed controller for PMSM has attracted much attention and many advanced methods have been proposed to address the above-mentioned drawbacks to achieve good speed control performance in recent years. A novel active disturbance rejection controller (ADRC) [13] is proposed to obtain the rapid dynamic response and strong anti-fluctuation performance. In [14], an optimized ADRC is proposed to achieve small overshoot, fast tracking, and strong anti-fluctuation performance. In this method, based on a new nonlinear function, various components of the ADRC are constructed. In [15], considering the complicated load fluctuation, a novel control approach based on the Lyapunov stability theory is presented to achieve good system stability. However, in [13]–[15], J and B are regarded as constants and the uncertainty of parameters is not considered. The parametric uncertainty leads to poor speed control performance in practical applications. In [16], an adaptive sliding mode control (SMC) method with a disturbance torque observer (DTO) is introduced to achieve speed control. In [17], on the basis

The associate editor coordinating the review of this manuscript and approving it for publication was Yonghong Peng.

of the nonsingular terminal sliding mode manifold, a novel nonsingular terminal SMC with a DTO is proposed for PMSM drive. Fast convergence and good tracking precision are achieved through this method. In [18], a SMC method combining a nonlinear fractional-order PID switching manifold, an extended state observer, and a super twisting reaching law is investigated to achieve small steady-state error, fast convergence, and strong anti-fluctuation performance. In [19], a speed control scheme with respect to a backstepping controller (BSPC) and a disturbance observer (DOB) is introduced to obtain strong anti-fluctuation performance. In this method, the nonlinear DOB is developed to estimate uncertain parameters and complicated load torque. In [20], a robust BSPC combining the integral term and the SMC method is studied for speed regulation to reduce the effect of parametric uncertainty and load fluctuation. In [21], based on the novel self-tuning law, an adaptive speed controller with strong robustness is proposed for speed regulation. The output feedback nonlinear H_∞ controller [22] is designed for PMSM to achieve strong robustness and anti-fluctuation performance. In [23], the model reference adaptive control (MRAC) approach with a compensating control term is introduced to achieve rapid speed response and strong robustness. The compensating control term is added for the uncertainty of PMSM parameters in this method. In [24]–[26], the model predictive control (MPC) method is utilized to obtain fast tracking performance and good anti-fluctuation performance. In [16]–[26], the complicated load fluctuation and the uncertainty of J and B are taken into account simultaneously, and the speed control performance is improved. However, there are many controller parameters with uncertainty and adjusting these parameters through trial and error is time-consuming. Additionally, the controller parameters obtained through trial and error are usually constants and not optimal for all work conditions, such as different speed conditions.

The intelligent control methods, such as the fuzzy control and the neural network (NN) control, are applied to the speed control of PMSM due to the strong capability of optimization and dealing with uncertain and nonlinear problems. In [27], based on the type-2 fuzzy logic control, an adaptive speed control approach is investigated to achieve accurate tracking and fast response. In [28]–[30], adaptive fuzzy output-feedback tracking control schemes combining fuzzy logic systems and the backstepping technique are investigated to reduce the effect of parametric uncertainty, unmodeled dynamics, and complicated load fluctuation. Fuzzy logic systems are used to approximate nonlinear functions and the backstepping technique is utilized to realize adaptive control in these methods. In [31], in order to deal with the parametric uncertainty and load fluctuation, the adaptive neuro-fuzzy inference system (ANFIS) is proposed for the speed regulation of PMSM. In [32], a robust dynamic output feedback control method with the Takagi-Sugeno (T-S) fuzzy model is utilized to reduce the effect of parametric uncertainty. However, in [27]–[32], the membership functions and fuzzy rules are mainly dependent on the extensive expert experience. It is difficult to obtain the extensive expert experience in practical applications. In [33], a speed control approach with a NN is proposed for the PMSM. The NN is utilized to identify the uncertain load and achieve the novel adaptive control. In [34], an adaptive neural finite-time tracking control scheme is developed to obtain accurate tracking. In this method, one NN is used to estimate the function with uncertain parameters and another NN is utilized to observe unavailable states. In [35], on the basis of the NN, a novel speed regulator for PMSM is studied to obtain good adaptive performance for uncertain parameters and fluctuant load. In this method, nonlinear functions are approximated through the NN. In [36], based on the recurrent Elman NN, a robust speed regulator is investigated to obtain high-performance control. Considering parametric uncertainty and load fluctuation, an intelligent and optimal recurrent wavelet-based Elman NN speed control scheme [37] is investigated to obtain fast response and good anti-fluctuation performance. In this method, the approximation of optimal control law is achieved by the NN. In [33]–[37], the speed control performance of PMSM is improved through the application of the NN, which is of great significance and provides much important guidance.

Among various NNs, the radial basis function NN (RBFNN) has been extensively applied to uncertain and complicated industrial control systems in recent years [38]–[41] due to the inherent characteristics of simple network structure, good approximation, fast learning speed, and strong generalization [42], [43]. In [40], a nonlinear current decoupling control scheme based on the RBFNN inverse system is presented. In [41], with consideration of uncertain PMSM parameters, an adaptive dynamic current decoupling control approach based on the RBFNN is developed to achieve strong decoupling performance. In [42], considering the parametric uncertainty, a sensorless speed control method based on the RBFNN is investigated for the induction motor. In this method, the RBFNN is used to estimate the speed in real time. In [43], in order to reduce the effect of the hydraulic power and load fluctuation on the linear motor-direct drive actuator system, the RBFNN is utilized to optimize controller parameters to achieve the novel adaptive control. However, for the SCS of PMSM, the studies in which the RBFNN is utilized to optimize control performance, and in which the complicated load fluctuation and uncertain J and B are considered simultaneously are rarely found. Inspired by these methods, the novel RBFNN is adopted to achieve novel speed regulation in this paper.

In this paper, a novel speed control scheme combining adaptive speed controller and RBFNN (ASC-RBFNN) is investigated for the SCS of PMSM to reduce the effect of parametric uncertainty and complicated load fluctuation. Compared with previous results, the main contributions of this paper are summarized as follows:

(1) On the basis of the Lyapunov stability theory and the dynamic motion equation considering parametric uncertainty and complicated load fluctuation, an ASC is designed to achieve the speed control.

(2) The SCS under the control of the proposed ASC is asymptotically stable even though J and B are uncertain and the complicated load fluctuation exists. Meanwhile, the ASC is with the characteristics of reducing the effect of complicated load fluctuation and the uncertainty of J and B on the speed control performance.

(3) With consideration of the uncertainty of complicated load, PMSM parameters, and ASC parameters, the novel RBFNN is used to optimize all ASC parameters for optimal speed control performance in whole-speed range.

The rest of the paper is organized as follows. In Section II, with consideration of parametric uncertainty and complicated load fluctuation, the mathematical model for PMSM is constructed. The asymptotically stable ASC is designed in Section III. The optimization of ASC parameters through the RBFNN is presented in Section IV. Experimental results are discussed in Section V and some conclusions are shown in Section VI.

II. MATHEMATICAL MODEL OF PMSM CONSIDERING PARAMETRIC UNCERTAINTY AND LOAD FLUCTUATION

To simplify analyses, four assumptions are made about PMSM: (1) The saturation of the magnetic circuit is not considered. (2) The hysteresis and eddy current loss are not considered. (3) The damper winding acting on the rotor is ignored. (4) The magnetic field is sinusoidal in space.

Additionally, J and B are uncertain due to various factors, including the inconsistent production, the mechanical wear, the change of the temperature, and the complicated work conditions [9]. The load is complicated and fluctuates due to the nonlinear friction and complicated work conditions [11].

According to the FOC theory [5] and above assumptions, the voltage equation and electromagnetic torque equation for PMSM with respect to d-q reference frame are represented as

$$\begin{cases} u_d = R_s i_d + L_d \dfrac{di_d}{dt} - \omega_e L_q i_q \\ u_q = R_s i_q + L_q \dfrac{di_q}{dt} + \omega_e L_d i_d + \omega_e \psi_f \end{cases} \tag{1}$$

$$T_e = \frac{3}{2} n_p \left[\psi_f i_q + \left(L_d - L_q \right) i_d i_q \right] \tag{2}$$

where u_d, i_d, and L_d are the stator voltage, stator current, and stator inductance of d-loop, respectively; u_q, i_q, and L_q are the stator voltage, stator current, and stator inductance of q-loop, respectively; and R_s, ψ_f, ω_e, T_e, and n_p are stator resistance, flux linkage of the permanent magnet, electrical angular velocity, electromagnetic torque, and the number of pole-pairs, respectively.

Meanwhile, the dynamic motion equation for PMSM considering parametric uncertainty and complicated load fluctuation is described as

$$\hat{J} \frac{d\omega}{dt} = T_e - \hat{B}\omega - \hat{T}_L \tag{3}$$

where ω is speed; $\hat{J}$ and $\hat{B}$ are the J and B with uncertainty; T_L is load torque; and $\hat{T}_L$ is the T_L with complicated load fluctuation.

Based on (1) to (3) and the FOC theory [5], the SCS of PMSM is with the double closed-loop control structure of an inner torque loop achieved by two current loops (d-loop and q-loop) and an outer speed loop, as shown in Fig. 1. In Fig. 1, ω^* is the reference value of ω. ASR is the conventional speed controller. The output of the ASR is T_e^* and is the reference input of the inner torque loop. i_d^* and i_q^* are the reference values of i_d and i_q, respectively. T_e^* is converted into i_d^* and i_q^* through the T-C module. In the T-C module, i_d^* is set through different modulation ratios and then i_q^* is calculated through (2), T_e^*, and i_d^*. ACR_d and ACR_q are the controllers of d-loop and q-loop, respectively. u_α and i_α are the voltage and current of α-axis, respectively. u_β and i_β are the voltage and current of β-axis, respectively. V_{dc} is the voltage of the DC bus. θ is electrical angle. i_A and i_B are the currents of A-axis and B-axis, respectively.

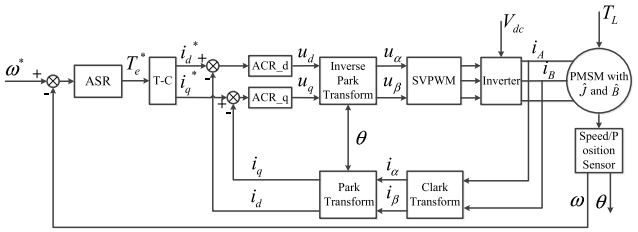

FIGURE 1. Block diagram of the SCS of PMSM.

In this paper, we focus on the outer speed loop and the design of the speed controller. In order to observe the characteristics of the outer speed loop more clearly and design the speed controller more conveniently, Fig. 1 is simplified, as shown in Fig. 2.

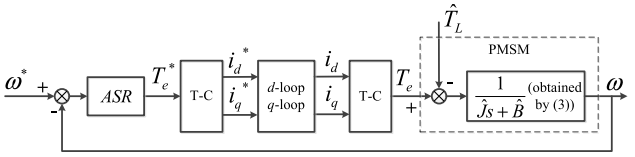

FIGURE 2. Structure diagram of the SCS of PMSM with time delay of torque.

In the double closed-loop control structure, there are corresponding control periods in the inner torque loop and the outer speed loop. In the inner torque loop, several control periods of the inner torque loop are required to achieve accurate torque tracking when T_e^* is changed [44], [45]. Thus the inner torque loop is equivalent to a time delay link of the outer speed loop. Furthermore, considering the loss of the inverter and PMSM, the control period of the inner torque loop is usually in the microsecond range. However, the time constant of PMSM is J/B and is usually in the millisecond range. Thus the time constant of PMSM is much larger than the time delay of torque. According to the dominant pole method, this time delay link is ignored in this paper. Therefore, Fig. 2 is simplified further, as shown in Fig. 3.

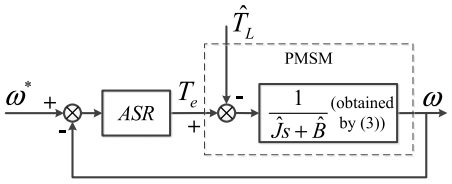

FIGURE 3. Structure diagram of the SCS of PMSM.

According to (3) and Fig. 3, it can be found that there are $\hat{J}$, $\hat{B}$, and $\hat{T}_L$ in the outer speed loop. The complicated load fluctuation and the uncertainty of motor parameters inevitably lead to poor system stability and large speed fluctuation.

III. DESIGN OF ASC

To reduce the effect of the complicated load fluctuation and the uncertainty of J and B on the speed control performance, an ASC is designed and is described as follows.

The speed error e between ω and ω^* is defined, as shown in

$$e = \omega^* - \omega \tag{4}$$

The reasons for the uncertainty are the inconsistent production, the mechanical wear, the change of the temperature, the nonlinear friction, and the complicated work conditions. If these factors are constant, $\hat{J}$, $\hat{B}$, and $\hat{T}_L$ are constants at all times. Thus, $\hat{J}$, $\hat{B}$, and $\hat{T}_L$ are considered as the functions of these factors and are not considered as the functions of time (t) in this paper.

Then, the derivative of e with respect to t is derived as

$$\dot{e} = \dot{\omega}^* - \dot{\omega} \tag{5}$$

A Lyapunov function is chosen in this paper, as shown in

$$V = \frac{1}{2}e^2 + \frac{1}{2}k_2\theta^2 > 0 \tag{6}$$

where V is a positive definite function; $k_2 > 0$ is the bounded gain; and

$$\theta = \int_0^t e\, dt \tag{7}$$

The derivative of V is derived as

$$\dot{V} = e\dot{e} + k_2 e\theta \tag{8}$$

Based on (3) and (5), (8) is rewritten as

$$\dot{V} = e\left[\dot{\omega}^* - \frac{T_e - \hat{B}\omega - \hat{T}_L}{\hat{J}} + k_2\theta\right] \tag{9}$$

With consideration of the stability of the SCS and the convergence of the e, a negative semi-definite $\dot{V}$ is needed. Thus, the ASC is designed, as shown in

$$T_e = \hat{J}\dot{\omega}^* + \hat{J}k_1 e + \hat{J}k_2\theta + \hat{B}\omega + \hat{T}_L \tag{10}$$

where $k_1 > 0$ is the bounded control gain.

According to (9) and (10), the negative semi-definite $\dot{V}$ is obtained, as shown in

$$\dot{V} = -k_1 e^2 \le 0 \tag{11}$$

Therefore, the SCS with the designed ASC is stable. Meanwhile, the ASC is adaptive for $\hat{J}$ and $\hat{B}$, and $\hat{T}_L$ in (10) is a compensation term for complicated load fluctuation. These characteristics are used to reduce the effect of complicated load fluctuation and the uncertainty of J and B on the speed control performance.

Furthermore, according to (6) and (11), V is a decreasing function and bounded, as shown in

$$0 < V \le V(0) \tag{12}$$

On the basis of (6), (12), and the boundedness of gain k_2, e and θ are bounded.

Based on (3), (5), (10), and the boundedness of e, θ, k_1, and k_2, $\dot{e}$ is bounded too and is rewritten as

$$\dot{e} = -k_1 e - k_2\theta \tag{13}$$

According to (11), the derivative of $\dot{V}$ is derived as

$$\ddot{V} = -2k_1 e\dot{e} \tag{14}$$

Due to the boundedness of $\dot{e}$, k_1, and e, $\ddot{V}$ is also bounded. Therefore, $\dot{V}$ is uniformly continuous.

Through the above analyses, it is concluded that: (1) $\dot{V}$ is negative semi-definite. (2) V is bounded. (3) $\dot{V}$ is uniformly continuous.

Based on the Barbalat Lemma [41], it can be found that

$$\lim_{t\to\infty} \dot{V} = 0 \tag{15}$$

Then, based on (15) and (11), it can be found that

$$\lim_{t\to\infty} e = 0 \tag{16}$$

Therefore, e approaches to 0 as t approaches to infinite, which means the SCS controlled by the ASC is asymptotically stable even though J and B are uncertain and the complicated load fluctuation exists.

Based on the above analyses and design, the following theorem is obtained.

Theorem 1: Suppose that the assumptions for establishing the mathematical model of PMSM hold and the time delay of torque is ignored. The SCS under the control of the proposed ASC is asymptotically stable even though J and B are uncertain and the complicated load fluctuation exists. Meanwhile, the ASC is with the characteristics of reducing the effect of complicated load fluctuation and the uncertainty of J and B on the speed control performance.

IV. OPTIMIZATION OF ASC PARAMETERS

There are $\hat{J}$, $\hat{B}$, $\hat{T}_L$, k_1, and k_2 in the ASC. k_1 and k_2 are uncertain since they need to be adjusted through trial and error. Meanwhile, $\hat{T}_L$ is also uncertain since it is determined by complicated work conditions. Considering the uncertainty

of complicated load, PMSM parameters, and ASC parameters, the RBFNN is used to optimize all ASC parameters for optimal speed control performance in whole-speed range.

Because the RBFNN is a numerical and iterative design method, a discrete ASC is required. Based on the backward difference operation, the discrete ASC is derived as

$$\begin{aligned} T_e(k+1) = y_1^3 \frac{\omega^*(k) - \omega^*(k-1)}{T} + y_2^3 e(k) \\ + y_3^3 T \sum\nolimits_{\mu=0}^{k} e(\mu) \\ + y_4^3 \omega(k) + y_5^3 \end{aligned} \tag{17}$$

where T and k are the control period and step size of the SCS, respectively; and

$$\begin{cases} y_1^3 = \hat{J} \\ y_2^3 = \hat{J} k_1 \\ y_3^3 = \hat{J} k_2 \\ y_4^3 = \hat{B} \\ y_5^3 = \hat{T}_L \end{cases} \tag{18}$$

The structure of the RBFNN is divided into three layers, as shown in Fig. 4.

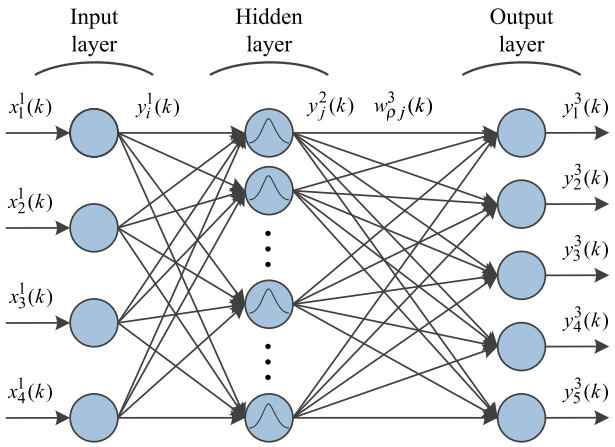

FIGURE 4. Structure of the RBFNN.

(1) The input layer consists of 4 source nodes. For each node, the signal propagation and output are represented as

$$net_i^1 = x_i^1, \quad i = 1, 2, 3, 4 \tag{19}$$

$$y_i^1(k) = f\left[\text{net}_i^1(k)\right] = net_i^1(k), \quad i = 1, 2, 3, 4 \tag{20}$$

The input vector of the network is represented as

$$\begin{aligned} \boldsymbol{x^1}(k) &= \left[x_1^1(k) \quad x_2^1(k) \quad x_3^1(k) \quad x_4^1(k)\right]^T \\ &= \left[\frac{\omega^*(k) - \omega^*(k-1)}{T} e(k) \quad T \sum\nolimits_{\mu=0}^{k} e(\mu) \quad \omega(k)\right]^T \end{aligned} \tag{21}$$

(2) The hidden layer consists of n nonlinear nodes. For each node, the radial basis function is chosen as the activation function. In the SCS of PMSM, it is difficult to obtain good training samples, which leads to the difficulty in obtaining the fixed and optimal center and width of each radial basis function through offline training and self-organizing learning methods, such as k-Means method. Meanwhile, PMSM is strongly nonlinear and uncertain, and the SCS of PMSM is complicated. The good approximation performance and control performance usually cannot be achieved through the fixed center and width. Considering above factors, both center and width of each radial basis function are iteratively learned and updated through the supervised learning method in this paper. The signal propagation and output are expressed as

$$net_j^2 = -\frac{\left\|\boldsymbol{x^1}(k) - \boldsymbol{c_j^2}(k)\right\|^2}{2b_j^2(k)^2}, j = 1, 2, \ldots, n \tag{22}$$

$$y_j^2(k) = g\left[net_j^2(k)\right] = \exp\left[net_j^2(k)\right], j = 1, 2, \ldots, n \tag{23}$$

where $\|\cdot\|$ is Euclidean distance function; $\boldsymbol{c_j^2}(k)$ and $b_j^2(k)$ are the center and width of the radial basis function of the j-th node, respectively; and $\boldsymbol{c_j^2}(k)$ is represented as

$$\boldsymbol{c_j^2}(k) = \left[c_{j1}^2(k) \; c_{j2}^2(k) \; c_{j3}^2(k) \; c_{j4}^2(k)\right]^T \tag{24}$$

The radial basis function vector of the network is represented as

$$\boldsymbol{y^2}(k) = \left[y_1^2(k) \; y_2^2(k) \; \cdots \; y_j^2(k) \; \cdots \; y_n^2(k)\right]^T \tag{25}$$

(3) The output layer consists of 5 linear nodes. For each node, the signal propagation and output are expressed as

$$net_\rho^3 = \sum\nolimits_{j=1}^{n} w_{\rho j}^3(k) y_j^2(k), \rho = 1, 2, 3, 4, 5 \tag{26}$$

$$y_\rho^3(k) = h\left[net_\rho^3(k)\right] = net_\rho^3(k), \rho = 1, 2, 3, 4, 5 \tag{27}$$

where $w_{\rho j}^3(k)$ is the weight between the j-th node of hidden layer and the ρ-th node of output layer.

The output vector of the network is represented as

$$\boldsymbol{y^3}(k) = \left[y_1^3(k) \; y_2^3(k) \; y_3^3(k) \; y_4^3(k) \; y_5^3(k)\right]^T \tag{28}$$

The cost function for the optimization of all ASC parameters is chosen as

$$E(k) = \frac{1}{2}\left[\omega^*(k) - \omega(k)\right]^2 \tag{29}$$

Then, according to the supervised learning method, back-propagation algorithm, and gradient descent method [34], all $w_{\rho j}^3(k)$, $c_{ji}^2(k)$, and $b_j^2(k)$ are iteratively learned and updated.

(1) For each $w^3_{\rho j}(k)$, the update rule is expressed as

$$w^3_{\rho j}(k) = w^3_{\rho j}(k-1) + \Delta w^3_{\rho j}(k) + \alpha[w^3_{\rho j}(k-1) - w^3_{\rho j}(k-2)], \quad \rho = 1,2,3,4,5; j = 1,2,\ldots,n \tag{30}$$

where $\alpha \in [0,1]$ is inertia term; $\eta \in [0,1]$ is learning rate; and

$$\begin{aligned}
&\Delta w^3_{\rho j}(k) \\
&= -\eta \frac{\partial E(k)}{\partial w^3_{\rho j}(k-1)} \\
&= -\eta \frac{\partial E(k)}{\partial \omega(k)} \frac{\partial \omega(k)}{\partial T_e(k)} \frac{\partial T_e(k)}{\partial y^3_\rho(k-1)} \frac{\partial y^3_\rho(k-1)}{\partial net^3_\rho(k-1)} \frac{\partial net^3_\rho(k-1)}{\partial w^3_{\rho j}(k-1)} \\
&= \eta e(k) \frac{\partial \omega(k)}{\partial T_e(k)} \frac{\partial T_e(k)}{\partial y^3_\rho(k-1)} y^2_j(k-1)
\end{aligned} \tag{31}$$

$$\frac{\partial \omega(k)}{\partial T_e(k)} = \operatorname{sgn}\left[\frac{\omega(k) - \omega(k-1)}{T_e(k) - T_e(k-1)}\right] \tag{32}$$

$$\frac{\partial T_e(k)}{\partial y^3_\rho(k-1)} = \begin{cases} [\omega^*(k-1) - \omega^*(k-2)]/T, & \rho = 1 \\ e(k-1), & \rho = 2 \\ T\sum_{\mu=0}^{k-1} e(\mu) & \rho = 3 \\ \omega(k-1), & \rho = 4 \\ 1, & \rho = 5 \end{cases} \tag{33}$$

(2) For each $c^2_{ji}(k)$, the update rule is represented as

$$c^2_{ji}(k) = c^2_{ji}(k-1) + \Delta c^2_{ji}(k) + \alpha[c^2_{ji}(k-1) - c^2_{ji}(k-2)], \quad j = 1,2,\ldots,n; i = 1,2,3,4 \tag{34}$$

where

$$\begin{aligned}
&\Delta c^2_{ji}(k) \\
&= -\eta \frac{\partial E(k)}{\partial c^2_{ji}(k-1)} \\
&= -\eta \frac{\partial E(k)}{\partial net^2_j(k-1)} \frac{\partial net^2_j(k-1)}{\partial c^2_{ji}(k-1)} \\
&= -\eta \frac{\partial E(k)}{\partial y^2_j(k-1)} \frac{\partial y^2_j(k-1)}{\partial net^2_j(k-1)} \frac{\partial net^2_j(k-1)}{\partial c^2_{ji}(k-1)}
\end{aligned} \tag{35}$$

$$\begin{aligned}
&\frac{\partial E(k)}{\partial y^2_j(k-1)} \\
&= \sum\nolimits_{\rho=1}^{5} \Big[\frac{\partial E(k)}{\partial \omega(k)} \frac{\partial \omega(k)}{\partial T_e(k)} \frac{\partial T_e(k)}{\partial y^3_\rho(k-1)} \frac{\partial y^3_\rho(k-1)}{\partial net^3_\rho(k-1)} \\
&\quad \times \frac{\partial net^3_\rho(k-1)}{\partial y^2_j(k-1)}\Big]
\end{aligned} \tag{36}$$

$$\begin{aligned}
&= \sum\nolimits_{\rho=1}^{5} \Big[\frac{\partial E(k)}{\partial \omega(k)} \frac{\partial \omega(k)}{\partial T_e(k)} \frac{\partial T_e(k)}{\partial y^3_\rho(k-1)} w^3_{\rho j}(k-1)\Big] \\
&\quad \frac{\partial y^2_j(k-1)}{\partial net^2_j(k-1)} \frac{\partial net^2_j(k-1)}{\partial c^2_{ji}(k-1)} \\
&= y^2_j(k-1) \frac{\left[x^1_i(k-1) - c^2_{ji}(k-1)\right]}{b^2_j(k-1)^2}
\end{aligned} \tag{37}$$

(3) For each $b^2_j(k)$, the update rule is represented as

$$b^2_j(k) = b^2_j(k-1) + \Delta b^2_j(k) + \alpha[b^2_j(k-1) - b^2_j(k-2)], j = 1,2,\ldots,n \tag{38}$$

where

$$\begin{aligned}
\Delta b^2_j(k) &= = -\eta \frac{\partial E(k)}{\partial b^2_j(k-1)} \\
&= -\eta \frac{\partial E(k)}{\partial net^2_j(k-1)} \frac{\partial net^2_j(k-1)}{\partial b^2_j(k-1)} \\
&= -\eta \frac{\partial E(k)}{\partial y^2_j(k-1)} \frac{\partial y^2_j(k-1)}{\partial net^2_j(k-1)} \frac{\partial net^2_j(k-1)}{\partial b^2_j(k-1)}
\end{aligned} \tag{39}$$

$$\begin{aligned}
&\frac{\partial y^2_j(k-1)}{\partial net^2_j(k-1)} \frac{\partial net^2_j(k-1)}{\partial b^2_j(k-1)} \\
&= y^2_j(k-1) \frac{\left\|\boldsymbol{x}^1(k-1) - \boldsymbol{c}^2_j(k-1)\right\|^2}{b^2_j(k-1)^3}
\end{aligned} \tag{40}$$

Based on the above analyses and design, the following theorem is obtained.

Theorem 2: Suppose that the assumptions for establishing the mathematical model of PMSM hold and the time delay of torque is ignored. All ASC parameters are optimized through the RBFNN shown above to obtain optimal speed control performance in whole-speed range. Meanwhile, the SCS of PMSM with the ASC-RBFNN scheme is shown in Fig. 5.

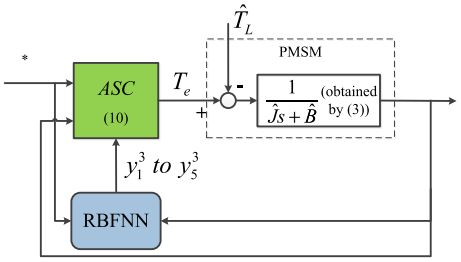

FIGURE 5. Structure diagram of the SCS of PMSM with ASC-RBFNN.

V. EXPERIMENTAL RESULTS

Aiming to observe the results and practicability of the ASC-RBFNN speed control scheme, an experiment platform of the SCS is set up, as shown in Fig. 6. In this experiment platform, motor parameters are shown in Table 1, load torque

TABLE 1. Parameters of PMSM.

Parameters	Value	Unit
Rated voltage	320	V
Rated torque	35	N·m
Rated speed	1000	rpm
Maximum torque	90	N·m
Maximum speed	3000	rpm
Number of pole-pairs	3	

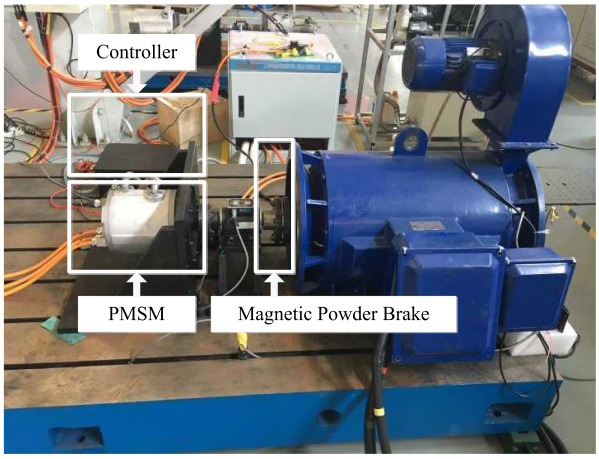

FIGURE 6. Experiment platform.

is adjusted by magnetic powder brake, and the ASC-RBFNN speed control scheme with the parameters of $n = 8$, $\alpha = 0.05$, and $\eta = 0.25$ is applied to the controller.

Additionally, in order to show the advantages, the results under the control of the ASC-RBFNN scheme and classical PI controller are compared. For a convincing and fair comparison, all PI parameters are adjusted repeatedly through experiments.

A. SPEED RESPONSE

To observe the speed response performance in whole-speed range, 500rpm (low speed), 1000rpm (rated speed), and 3000rpm (maximum speed) are chosen as the step reference speed. In each step reference speed condition, comparative experiments are carried out. The response curves of the ASC-RBFNN speed control scheme and the PI controller in each step reference speed condition are shown in Fig. 7 to Fig. 9.

Fig. 7 shows response curves when the step reference speed is 500rpm. At $t = 0$, the reference speed is changed from 0 to 500rpm. Then the motor speed starts to rise and the motor works in dynamic. Firstly, there is no speed overshoot in both methods. Secondly, the settling time of speed, T_e, and i_q^* is close and is about 0.18s under the control of the PI controller. The maximum values of T_e and i_q^* are about 28.2N·m and 14.6A, respectively. However, the settling time of speed, T_e, and i_q^* is close and is about 0.04s under the control of the ASC-RBFNN scheme. The maximum values of

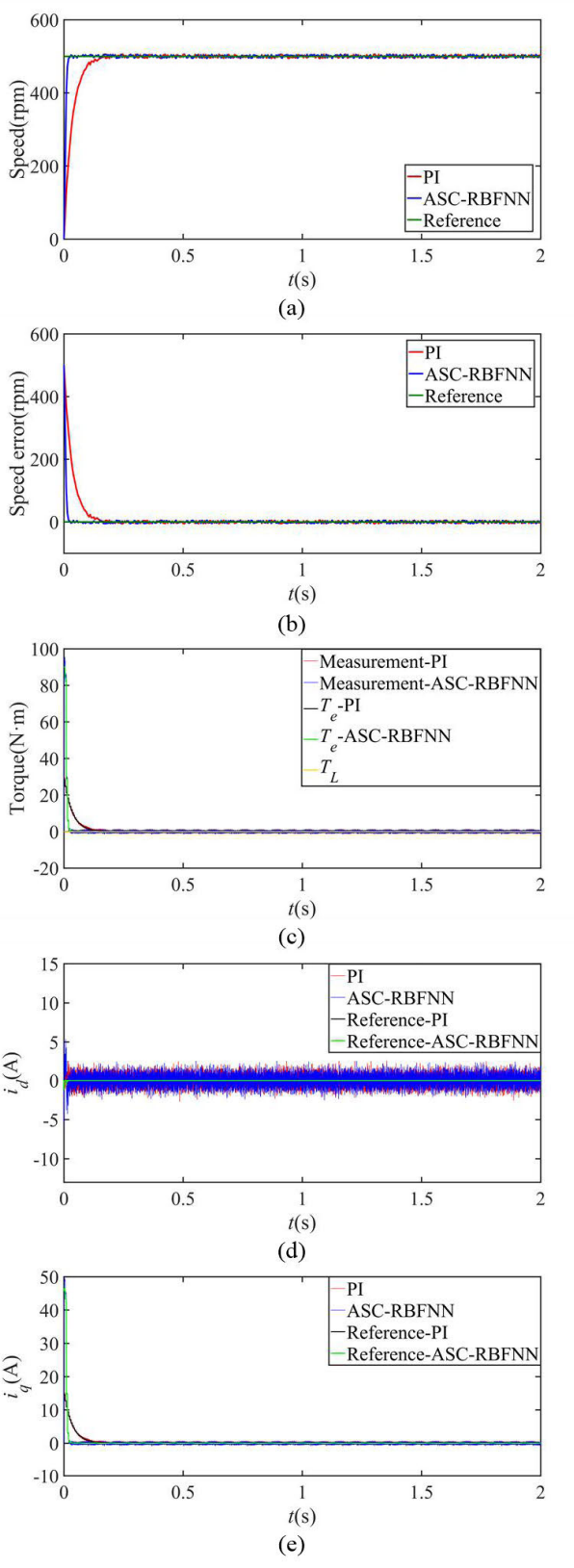

FIGURE 7. Response curves in the step reference speed of 500rpm. (a) Speed response curves. (b) Speed error curves. (c) Torque response curves. (d) i_d response curves. (e) i_q response curves.

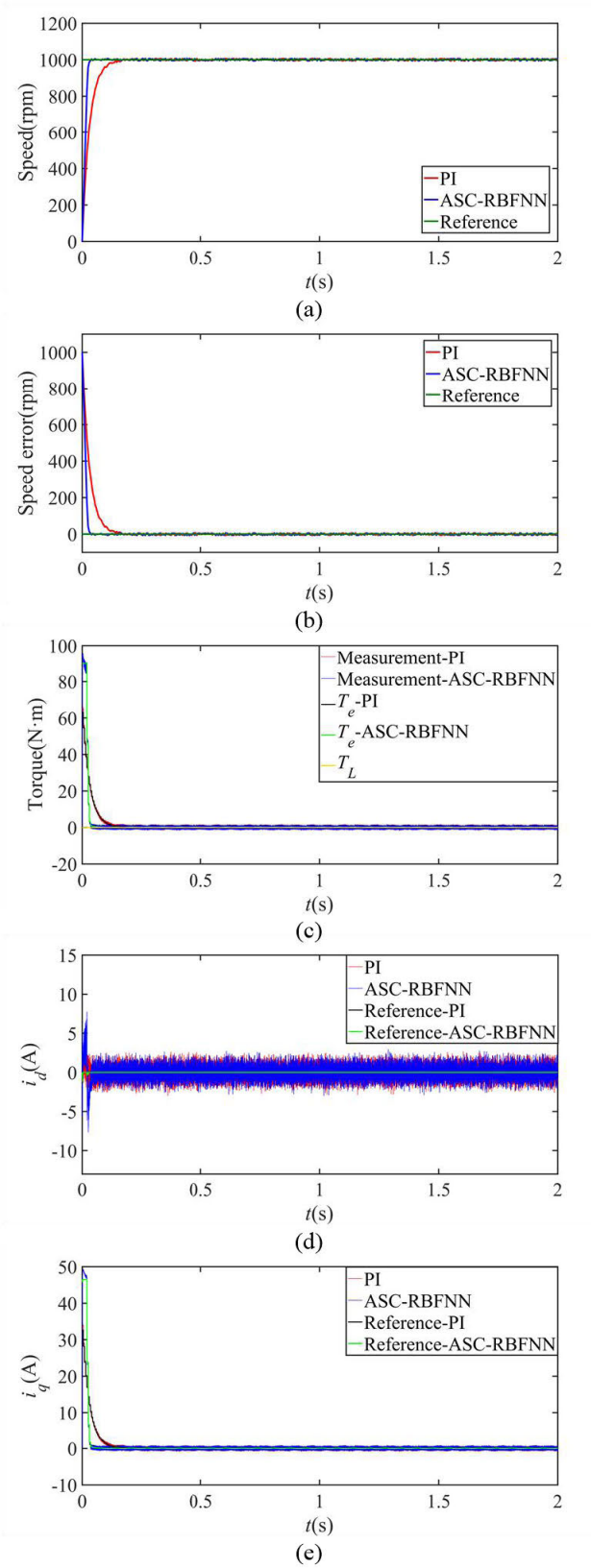

FIGURE 8. Response curves in the step reference speed of 1000rpm. (a) Speed response curves. (b) Speed error curves. (c) Torque response curves. (d) i_d response curves. (e) i_q response curves.

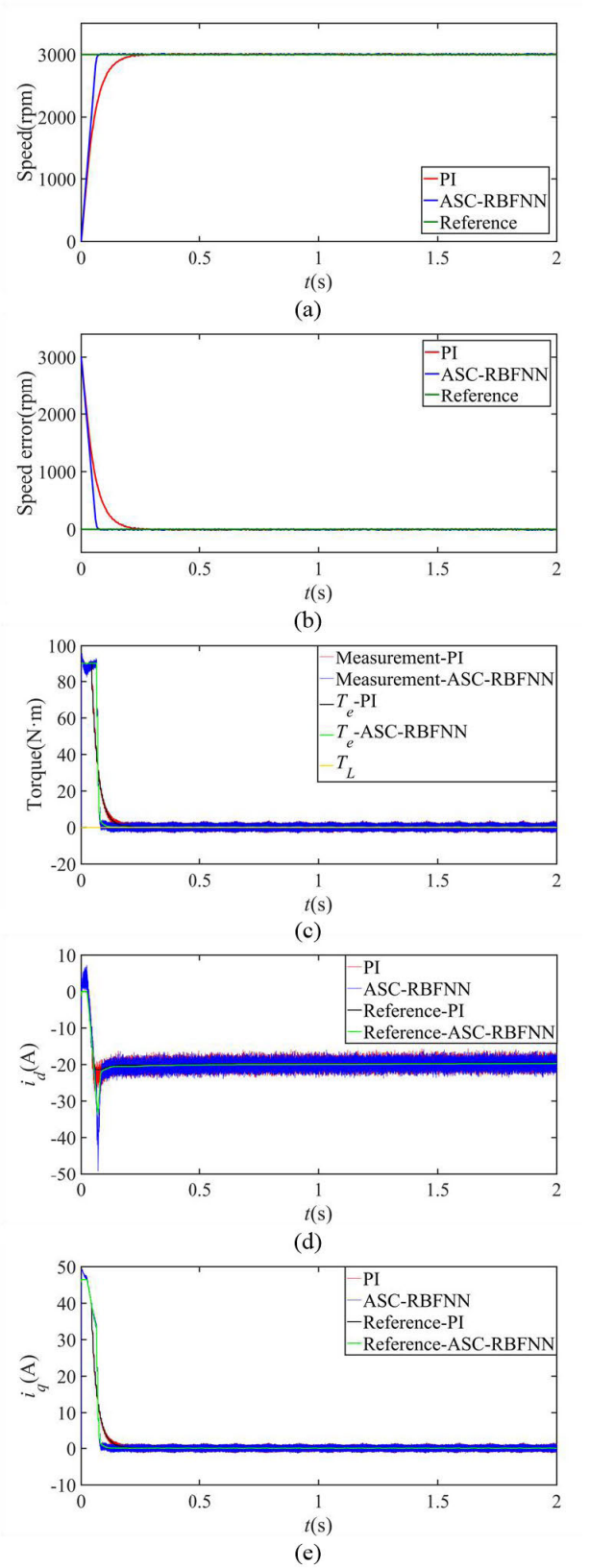

FIGURE 9. Response curves in the step reference speed of 3000rpm. (a) Speed response curves. (b) Speed error curves. (c) Torque response curves. (d) i_d response curves. (e) i_q response curves.

T_e and i_q^* are about 90 N·m and 46.5A, respectively. Thirdly, i_d^* is 0 in both methods. The fluctuation of i_d is about ±3.1A under the control of the PI controller and is about ±4.5A under the control of the ASC-RBFNN scheme. Although the fluctuation of i_d of the ASC-RBFNN scheme is larger than that of the PI controller, ±4.5A is acceptable in actual applications. In Fig. 7, when the motor works in steady state, speed, the measurement of the torque in the experiment platform, i_d, and i_q track respective reference values accurately with small fluctuation of ±4.5rpm, ±1.3N·m, ±2.5A, and ±0.7A, respectively.

Fig. 8 shows response curves when the step reference speed is 1000rpm. At $t = 0$, the reference speed is changed from 0 to 1000rpm. Then the motor speed starts to rise and the motor works in dynamic. Firstly, there is no speed overshoot in both methods. Secondly, the settling time of speed, T_e, and i_q^* is close and is about 0.21s under the control of the PI controller. The maximum values of T_e and i_q^* are about 63.1N·m and 32.6A, respectively. However, the settling time of speed, T_e, and i_q^* is close and is about 0.05s under the control of the ASC-RBFNN scheme. The maximum values of T_e and i_q^* are about 90N·m and 46.5A, respectively. Thirdly, i_d^* is 0 in both methods. The fluctuation of i_d is about ±5.2A under the control of the PI controller and is about ±7.5A under the control of the ASC-RBFNN scheme. Although the fluctuation of i_d of the ASC-RBFNN scheme is larger than that of the PI controller, ±7.5A is acceptable in actual applications. In Fig. 8, when the motor works in steady state, speed, the measurement of the torque in the experiment platform, i_d, and i_q track respective reference values accurately with small fluctuation of ±5.8rpm, ±1.5N·m, ±2.7A, and ±0.8A, respectively.

Fig. 9 shows response curves when the step reference speed is 3000rpm. At $t = 0$, the reference speed is changed from 0 to 3000rpm. Then the motor speed starts to rise, and the motor works in dynamic. Firstly, there is no speed overshoot in both methods. Secondly, the settling time of speed, T_e, and i_q^* is close and is about 0.23s under the control of the PI controller. However, the settling time of speed, T_e, and i_q^* is close and is about 0.08s under the control of the ASC-RBFNN scheme. The maximum values of T_e and i_q^* are about 90N·m and 46.5A in both methods. However, the duration of the maximum torque of the ASC-RBFNN scheme is longer than that of the PI controller. Thirdly, i_d^* is less than 0 and the motor works in the field weakening area in both methods. The minimum value of i_d^* is about -40A under the control of the ASC-RBFNN scheme and is about -21.5A under the control of the PI controller. In Fig. 9, when the motor works in steady state, speed, the measurement of the torque in the experiment platform, i_d, and i_q track respective reference values accurately with small fluctuation of ±8.5rpm, ±3.5N·m, ±3.5A, and ±1.5A, respectively.

Therefore, the SCS controlled by the ASC-RBFNN scheme is with good system stability. Meanwhile, the speed response of the ASC-RBFNN is faster than that of the classical PI controller and the proposed ASC-RBFNN scheme is with fast speed response in whole-speed range.

B. ANTI-FLUCTUATION PERFORMANCE

To observe the anti-fluctuation performance in whole-speed range, firstly, the motor is operated in 500rpm, 1000rpm, and 3000rpm conditions, respectively. Then, in each speed condition, the load torque is changed from 0 to 30N·m suddenly at $t = 0.5$s and from 30N·m to 0 suddenly at $t = 1.5$s. The response curves of the ASC-RBFNN control scheme and the classical PI controller in different speed conditions are shown in Fig. 10 to Fig. 12.

Fig. 10 shows response curves under load fluctuation when the speed is 500rpm. When the load torque is changed suddenly, the motor works in dynamic. Firstly, the speed fluctuation and the recovery time under the control of the PI controller are about 190.2rpm and 0.48s, respectively. However, the speed fluctuation and the recovery time under the control of the ASC-RBFNN scheme are about 25.8rpm and 0.07s, respectively. Secondly, the settling time of T_e and i_q^* is close and is about 0.48s under the control of the PI controller. However, the settling time of T_e and i_q^* is close and is about 0.07s under the control of the ASC-RBFNN scheme. Thirdly, i_d^* is 0 in both methods. The fluctuation of i_d is about ±2.8A under the control of the PI controller and is about ±3.4A under the control of the ASC-RBFNN scheme. Although the fluctuation of i_d of the ASC-RBFNN scheme is larger than that of the PI controller, ±3.4A is acceptable in actual applications. In Fig. 10, when the motor works in steady state and the load torque is 0, speed, the measurement of the torque in the experiment platform, i_d, and i_q track respective reference values accurately with small fluctuation of ±4.5rpm, ±1.3N·m, ±2.5A, and ±0.7A, respectively. When the motor works in steady state and the load torque is 30N·m, speed, the measurement of the torque in the experiment platform, i_d, and i_q track respective reference values accurately with small fluctuation of ±5.4rpm, ±1.8N·m, ±2.8A, and ±0.9A, respectively.

Fig. 11 shows response curves under load fluctuation when the speed is 1000rpm. When the load torque is changed suddenly, the motor works in dynamic. Firstly, the speed fluctuation and the recovery time under the control of the PI controller are about 191.3rpm and 0.41s, respectively. However, the speed fluctuation and the recovery time under the control of the ASC-RBFNN scheme are about 25.4rpm and 0.05s, respectively. Secondly, the settling time of T_e and i_q^* is close and is about 0.41s under the control of the PI controller. However, the settling time of T_e and i_q^* is close and is about 0.05s under the control of the ASC-RBFNN scheme. Thirdly, i_d^* is 0 in both methods. The fluctuation of i_d is about ±3A under the control of the PI controller and is about ±4.6A under the control of the ASC-RBFNN scheme. Although the fluctuation of i_d of the ASC-RBFNN scheme is larger than that of the PI controller, ±4.6A is acceptable in actual applications. In Fig. 11, when the motor works in steady state and the load torque is 0, speed, the measurement of the torque

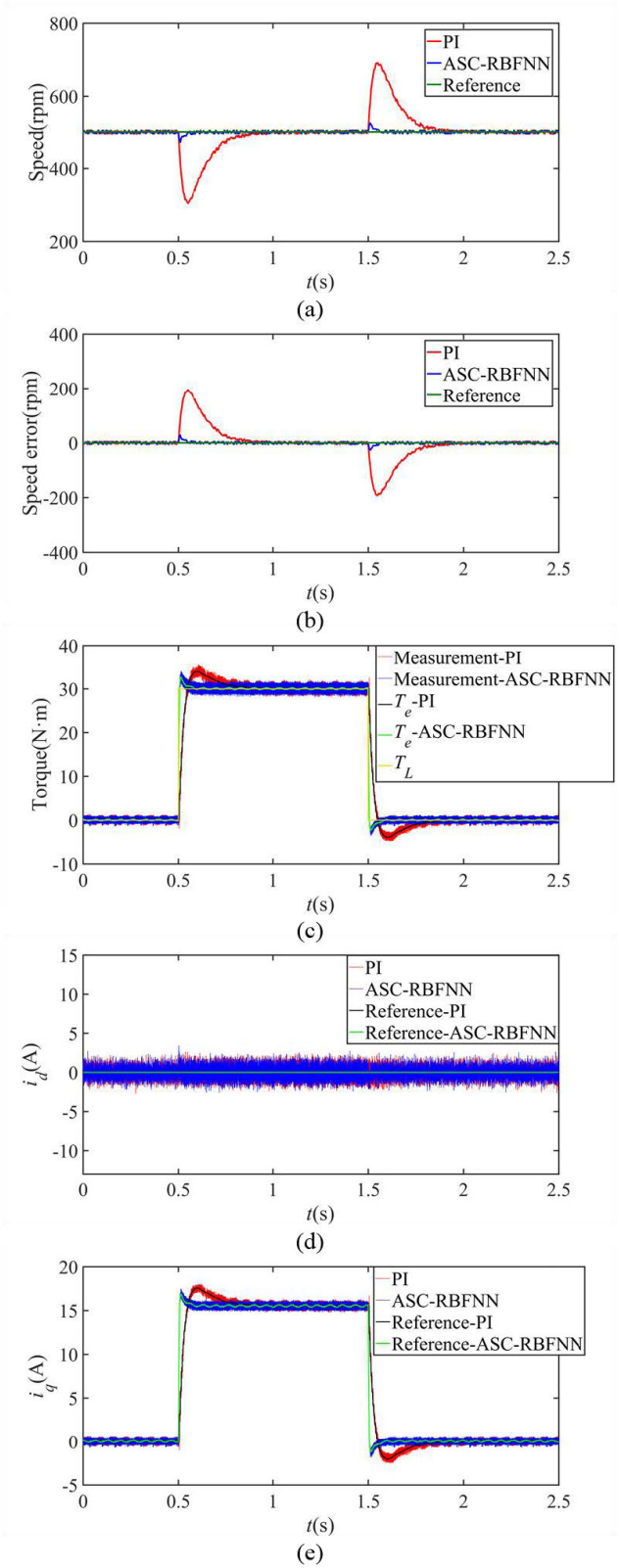

FIGURE 10. Response curves under load fluctuation when the speed is 500rpm. (a) Speed response curves. (b) Speed error curves. (c) Torque response curves. (d) i_d response curves. (e) i_q response curves.

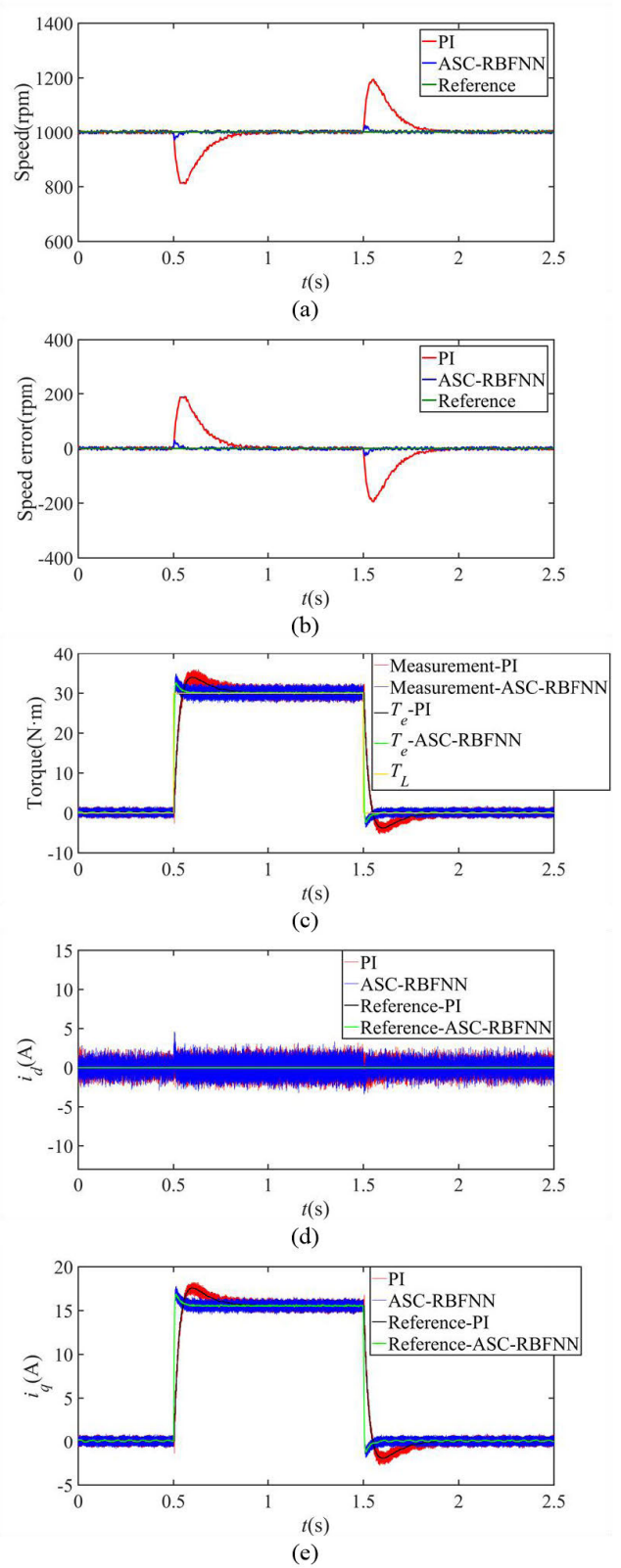

FIGURE 11. Response curves under load fluctuation when the speed is 1000rpm. (a) Speed response curves. (b) Speed error curves. (c) Torque response curves. (d) i_d response curves. (e) i_q response curves.

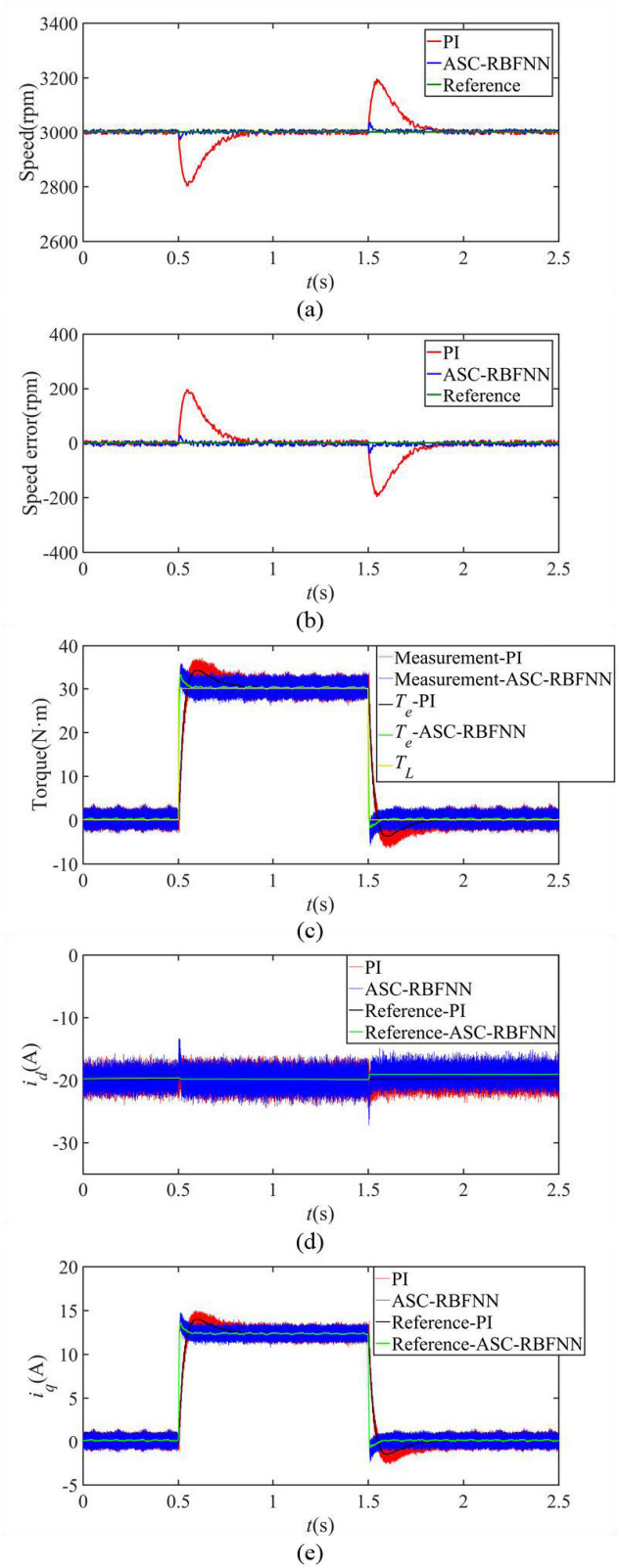

FIGURE 12. Response curves under load fluctuation when the speed is 3000rpm. (a) Speed response curves. (b) Speed error curves. (c) Torque response curves. (d) i_d response curves. (e) i_q response curves.

in the experiment platform, i_d, and i_q track respective reference values accurately with small fluctuation of ±5.8rpm, ±1.5N·m, ±2.7A, and ±0.8A, respectively. When the motor works in steady state and the load torque is 30N·m, speed, the measurement of the torque in the experiment platform, i_d, and i_q track respective reference values accurately with small fluctuation of ±6.8rpm, ±2.5N·m, ±3A, and ±1.1A, respectively.

Fig. 12 shows response curves under load fluctuation when the speed is 3000rpm. When the load torque is changed suddenly, the motor works in dynamic. Firstly, the speed fluctuation and the recovery time under the control of the PI controller are about 192rpm and 0.33s, respectively. However, the speed fluctuation and the recovery time under the control of the ASC-RBFNN scheme are about 27rpm and 0.03s, respectively. Secondly, the settling time of T_e and i_q^* is close and is about 0.33s under the control of the PI controller. However, the settling time of T_e and i_q^* is close and is about 0.03s under the control of the ASC-RBFNN scheme. Thirdly, i_d^* is about -19.8A and the motor works in the field weakening area in both methods. The fluctuation of i_d is about ±4.4A under the control of the PI controller and is about ±6.5A under the control of the ASC-RBFNN scheme. Although the fluctuation of i_d of the ASC-RBFNN scheme is larger than that of the PI controller, ±6.5A is acceptable in actual applications. In Fig. 12, when the motor works in steady state and the load torque is 0, the motor works in the field weakening area in both methods. Meanwhile, speed, the measurement of the torque in the experiment platform, i_d, and i_q track respective reference values accurately with small fluctuation of ±8.5rpm, ±3.5N·m, ±3.5A, and ±1.5A, respectively. When the motor works in steady state and the load torque is 30N·m, the motor works in the field weakening area in both methods. Meanwhile, speed, the measurement of the torque in the experiment platform, i_d, and i_q track respective reference values accurately with small fluctuation of ±9.5rpm, ±3.9N·m, ±4A, and ±1.6A, respectively.

Therefore, the SCS controlled by the ASC-RBFNN scheme is with good system stability and strong anti-fluctuation performance in whole-speed range.

In a word, all results indicate that the SCS controlled by the ASC-RBFNN speed control scheme is with good system stability, fast speed response, and strong anti-fluctuation performance in whole-speed range.

VI. CONCLUSION

The complicated load fluctuation and the uncertainty of J and B lead to poor system stability and large speed fluctuation. Therefore, a novel ASC-RBFNN speed control scheme is investigated in this paper. Firstly, with consideration of parametric uncertainty and complicated load fluctuation, the dynamic motion equation of PMSM is presented. Secondly, a positive definite Lyapunov function V is constructed

and an asymptotically stable ASC is designed through constructing a negative semi-definite $\dot{V}$. Meanwhile, the ASC is with the characteristics of reducing the effect of parametric uncertainty and complicated load fluctuation on the speed control performance. Thirdly, the RBFNN is used to optimize all ASC parameters for optimal speed control performance. Finally, many comparative experiments are carried out and the experimental results indicate that good system stability, fast speed response, and strong anti-fluctuation performance in whole-speed range are achieved through the ASC-RBFNN speed control scheme.

It should be pointed out that the design method of the controller in this paper can be applied to other control systems with uncertain parameters and complex load disturbances. Additionally, according to the results of this paper, relevant research is worthy to be studied in future work. Firstly, the novel load observer (LOB) or DOB can be investigated and added to reduce the effect of complicated load fluctuation further. The parameters of LOB or DOB can be optimized through NN for optimal estimation performance. Secondly, the performance of different intelligent algorithms can be compared.

REFERENCES

[1] Q. Fei, Y. Deng, H. Li, J. Liu, and M. Shao, "Speed ripple minimization of permanent magnet synchronous motor based on model predictive and iterative learning controls," *IEEE Access*, vol. 7, pp. 31791–31800, 2019.

[2] Y. Cho, K.-B. Lee, J.-H. Song, and Y. I. Lee, "Torque-ripple minimization and fast dynamic scheme for torque predictive control of permanent-magnet synchronous motors," *IEEE Trans. Power Electron.*, vol. 30, no. 4, pp. 2182–2190, Apr. 2015.

[3] H. Chaoui, M. Khayamy, and O. Okoye, "Adaptive RBF network based direct voltage control for interior PMSM based vehicles," *IEEE Trans. Veh. Technol.*, vol. 67, no. 7, pp. 5740–5749, Jul. 2018.

[4] J. Lara, J. Xu, and A. Chandra, "Effects of rotor position error in the performance of field-oriented-controlled PMSM drives for electric vehicle traction applications," *IEEE Trans. Ind. Electron.*, vol. 63, no. 8, pp. 4738–4751, Aug. 2016.

[5] P. Pillay and R. Krishnan, "Modeling of permanent magnet motor drives," *IEEE Trans. Ind. Electron.*, vol. IE-35, no. 4, pp. 537–541, Nov. 1988.

[6] A. Wang, Q. Wang, and W. Jiang, "A novel double-loop vector control strategy for PMSMs based on kinetic energy feedback," *J. Power Electron.*, vol. 15, no. 5, pp. 1256–1263, Sep. 2015.

[7] B. Xu, X. Shen, W. Ji, G. Shi, J. Xu, and S. Ding, "Adaptive nonsingular terminal sliding model control for permanent magnet synchronous motor based on disturbance observer," *IEEE Access*, vol. 6, pp. 48913–48920, 2018.

[8] P. Pillay and R. Krishnan, "Modeling, simulation, and analysis of permanent-magnet motor drives. I. The permanent-magnet synchronous motor drive," *IEEE Trans. Ind. Appl.*, vol. 25, no. 2, pp. 265–273, Apr. 1989.

[9] Z.-H. Liu, H.-L. Wei, X.-H. Li, K. Liu, and Q.-C. Zhong, "Global identification of electrical and mechanical parameters in PMSM drive based on dynamic self-learning PSO," *IEEE Trans. Power Electron.*, vol. 33, no. 12, pp. 10858–10871, Dec. 2018.

[10] X. Zhang and Z. Li, "Sliding-mode observer-based mechanical parameter estimation for permanent magnet synchronous motor," *IEEE Trans. Power Electron.*, vol. 31, no. 8, pp. 5732–5745, Aug. 2016.

[11] X. Sun, H. Yu, J. Yu, and X. Liu, "Design and implementation of a novel adaptive backstepping control scheme for a PMSM with unknown load torque," *IET Electr. Power Appl.*, vol. 13, no. 4, pp. 445–455, Apr. 2019.

[12] X. Liu, H. Yu, J. Yu, and L. Zhao, "Combined speed and current terminal sliding mode control with nonlinear disturbance observer for PMSM drive," *IEEE Access*, vol. 6, pp. 29594–29601, 2018.

[13] K. Zhou, M. Ai, Y. Sun, X. Wu, and R. Li, "PMSM vector control strategy based on active disturbance rejection controller," *Energies*, vol. 12, no. 20, p. 3827, Oct. 2019.

[14] Y. Meng, B. Liu, and L. Wang, "Speed control of PMSM based on an optimized ADRC controller," *Math. Problems Eng.*, vol. 2019, May 2019, Art. no. 1074702.

[15] M. Ouassaid, M. Cherkaoui, A. Nejmi, and M. Maaroufi, "Nonlinear torque control for PMSM: A Lyapunov technique," in *Proc. World Acad. Sci., Eng. Technol.*, vol. 6, Jun. 2005, pp. 118–121.

[16] Q. Wang, H. Yu, M. Wang, and X. Qi, "An improved sliding mode control using disturbance torque observer for permanent magnet synchronous motor," *IEEE Access*, vol. 7, pp. 36691–36701, 2019.

[17] S. Li, M. Zhou, and X. Yu, "Design and implementation of terminal sliding mode control method for PMSM speed regulation system," *IEEE Trans. Ind. Informat.*, vol. 9, no. 4, pp. 1879–1891, Nov. 2013.

[18] P. Gao, G. Zhang, H. Ouyang, and L. Mei, "An adaptive super twisting nonlinear fractional order PID sliding mode control of permanent magnet synchronous motor speed regulation system based on extended state observer," *IEEE Access*, vol. 8, pp. 53498–53510, 2020.

[19] X.-D. Liu, K. Li, and C.-H. Zhang, "Improved backstepping control with nonlinear disturbance observer for the speed control of permanent magnet synchronous motor," *J. Electr. Eng. Technol.*, vol. 14, no. 1, pp. 275–285, Jan. 2019.

[20] S. Wu and J. Zhang, "A terminal sliding mode observer based robust backstepping sensorless speed control for interior permanent magnet synchronous motor," *Int. J. Control, Autom. Syst.*, vol. 16, no. 6, pp. 2743–2753, Dec. 2018.

[21] S.-K. Kim, "Robust adaptive speed regulator with self-tuning law for surfaced-mounted permanent magnet synchronous motor," *Control Eng. Pract.*, vol. 61, pp. 55–71, Apr. 2017.

[22] R. Ramírez-Villalobos, L. T. Aguilar, and L. N. Coria, "Sensorless H-infinity speed-tracking synthesis for surface-mount permanent magnet synchronous motor," *ISA Trans.*, vol. 67, pp. 140–150, Mar. 2017.

[23] A. T. Nguyen, M. S. Rafaq, H. H. Choi, and J.-W. Jung, "A model reference adaptive control based speed controller for a surface-mounted permanent magnet synchronous motor drive," *IEEE Trans. Ind. Electron.*, vol. 65, no. 12, pp. 9399–9409, Dec. 2018.

[24] X. Zhang, Y. Cheng, Z. Zhao, and Y. He, "Robust model predictive direct speed control for SPMSM drives based on full parameter disturbances and load observer," *IEEE Trans. Power Electron.*, vol. 35, no. 8, pp. 8361–8373, Aug. 2020.

[25] M. Shao, Y. Deng, H. Li, J. Liu, and Q. Fei, "Robust speed control for permanent magnet synchronous motors using a generalized predictive controller with a high-order terminal sliding-mode observer," *IEEE Access*, vol. 7, pp. 121540–121551, 2019.

[26] J. Rodriguez and P. Cortes, "Predictive control of permanent magnet synchronous motors," in *Predictive Control of Power Converters and Electrical Drives*. Hoboken, NJ, USA: Wiley, 2012, ch. 9, pp. 133–144, doi: 10.1002/9781119941446.

[27] H. Chaoui, M. Khayamy, and A. A. Aljarboua, "Adaptive interval type-2 fuzzy logic control for PMSM drives with a modified reference frame," *IEEE Trans. Ind. Electron.*, vol. 64, no. 5, pp. 3786–3797, May 2017.

[28] L. Ma, X. Huo, X. Zhao, and G. Zong, "Adaptive fuzzy tracking control for a class of uncertain switched nonlinear systems with multiple constraints: A small-gain approach," *Int. J. Fuzzy Syst.*, vol. 21, no. 8, pp. 2609–2624, Oct. 2019.

[29] Y. Chang, Y. Wang, F. E. Alsaadi, and G. Zong, "Adaptive fuzzy output-feedback tracking control for switched stochastic pure-feedback nonlinear systems," *Int. J. Adapt. Control*, vol. 33, no. 10, pp. 1567–1582, Oct. 2019.

[30] Y. Wang, Y. Chang, A. F. Alkhateeb, and N. D. Alotaibi, "Adaptive fuzzy output-feedback tracking control for switched nonstrict-feedback nonlinear systems with prescribed performance," *Circuits, Syst., Signal Process.*, early access, Jun. 2020, doi: 10.1007/s00034-020-01466-y.

[31] R. Shanthi, S. Kalyani, and P. M. Devie, "Design and performance analysis of adaptive neuro-fuzzy controller for speed control of permanent magnet synchronous motor drive," *Soft Comput.*, early access, Aug. 2020, doi: 10.1007/s00500-020-05236-5.

[32] X.-H. Chang, J. Xiong, and J. H. Park, "Fuzzy robust dynamic output feedback control of nonlinear systems with linear fractional parametric uncertainties," *Appl. Math. Comput.*, vol. 291, pp. 213–225, Dec. 2016.

[33] M. A. Rahman and M. A. Hoque, "On-line adaptive artificial neural network based vector control of permanent magnet synchronous motors," *IEEE Trans. Energy Convers.*, vol. 13, no. 4, pp. 311–318, Dec. 1998.

[34] L. Ma, G. Zong, X. Zhao, and X. Huo, "Observed-based adaptive finite-time tracking control for a class of nonstrict-feedback nonlinear systems with input saturation," *J. Franklin Inst.*, vol. 357, pp. 1–27, Jul. 2019, doi: 10.1016/j.jfranklin.2019.07.021.
[35] J. Yu, P. Shi, W. Dong, B. Chen, and C. Lin, "Neural network-based adaptive dynamic surface control for permanent magnet synchronous motors," *IEEE Trans. Neural Netw. Learn. Syst.*, vol. 26, no. 3, pp. 640–645, Mar. 2015.
[36] R. Jon, Z. Wang, C. Luo, and M. Jong, "Adaptive robust speed control based on recurrent elman neural network for sensorless PMSM servo drives," *Neurocomputing*, vol. 227, pp. 131–141, Mar. 2017.
[37] F. F. M. El-Sousy, "Intelligent optimal recurrent wavelet elman neural network control system for permanent-magnet synchronous motor servo drive," *IEEE Trans. Ind. Informat.*, vol. 9, no. 4, pp. 1986–2003, Nov. 2013.
[38] Y. Wang, Q. Lin, X. Wang, and F. Zhou, "Adaptive PD control based on RBF neural network for a wire-driven parallel robot and prototype experiments," *Math. Problems Eng.*, vol. 2019, Feb. 2019, Art. no. 6478506.
[39] F. F. M. El-Sousy, "Adaptive dynamic sliding-mode control system using recurrent RBFN for high-performance induction motor servo drive," *IEEE Trans. Ind. Informat.*, vol. 9, no. 4, pp. 1922–1936, Nov. 2013.
[40] Y. Li, B. Li, X. Xu, and X. Sun, "A nonlinear decoupling control approach using RBFNNI-based robust pole placement for a permanent magnet in-wheel motor," *IEEE Access*, vol. 6, pp. 1844–1854, 2018.
[41] H. Jie, G. Zheng, J. Zou, X. Xin, and L. Guo, "Adaptive decoupling control using radial basis function neural network for permanent magnet synchronous motor considering uncertain and time-varying parameters," *IEEE Access*, vol. 8, pp. 112323–112332, 2020.
[42] P. Brandstetter and M. Kuchar, "Sensorless control of variable speed induction motor drive using RBF neural network," *J. Appl. Log.*, vol. 24, pp. 97–108, Nov. 2017.
[43] Z. Liu and T. Chen, "RBF neural network control for linear motor-direct drive actuator based on an extended state observer," *Discrete Dyn. Nature Soc.*, vol. 2016, Oct. 2016, Art. no. 8390529.
[44] B. Wang, W. Chen, B. Zhang, and Y. Zhao, "Regulation cooperative control for heterogeneous uncertain chaotic systems with time delay: A synchronization errors estimation framework," *Automatica*, vol. 108, Oct. 2019, Art. no. 108486, doi: 10.1016/j.automatica.2019.06.038.
[45] C. Deng and C. Wen, "MAS-based distributed resilient control for a class of cyber-physical systems with communication delays under DoS attacks," *IEEE Trans. Cybern.*, early access, Mar. 3, 2020, doi: 10.1109/TCYB.2020.2972686.

HONGYU JIE was born in Hohhot, China, in 1992. He received the B.S. degree in automation from UESTC, Chengdu, China, in 2014, where he is currently pursuing the Ph.D. degree. His research interests include motor drive systems, adaptive control, intelligent control, and electric vehicle control.

GANG ZHENG was born in Chengdu, Sichuan, China, in 1980. He received the Ph.D. degree in automation from UESTC, Chengdu, in 2011. His research interests include wind power systems and electric ship propulsion systems.

JIANXIAO ZOU (Member, IEEE) was born in Nanchang, Jiangxi, China, in 1978. He received the Ph.D. degree in automation from UESTC, Chengdu, China, in 2009. He is currently a Professor with the School of Automation Engineering, UESTC. His research interests include power electronics and renewable power generation systems and control technologies.

XIAOSHUAI XIN was born in Zhengzhou, Henan, China, in 1983. He received the Ph.D. degree in automation from UESTC, Chengdu, China, in 2014. His research interests include robust control and optimal control for motor and electric vehicles.

LUOLE GUO was born in Dazhou, Sichuan, China, in 1989. He received the M.S. degree in automation from UESTC, Chengdu, China, in 2012, where he is currently pursuing the Ph.D. degree. His research interests include adaptive control and intelligent control for motor.